RSC Advances

ROYAL SOCIETY OF CHEMISTRY

www.rsc.org/advances

Highlight:

Cu-SSZ-13 crystallized for 72 h shows excellent hydrothermal stability, NO_x removal activity and N_2 selectivity even under high space velocity (640,000 h^{-1}).

Aging treatments lead to the transform of copper species from isolated Cu^{2+} to new complexes.

Aging treatments lead to the dealuminization of the zeolites framework, which contributes to the catalyst deactivation.

Graphical abstract:

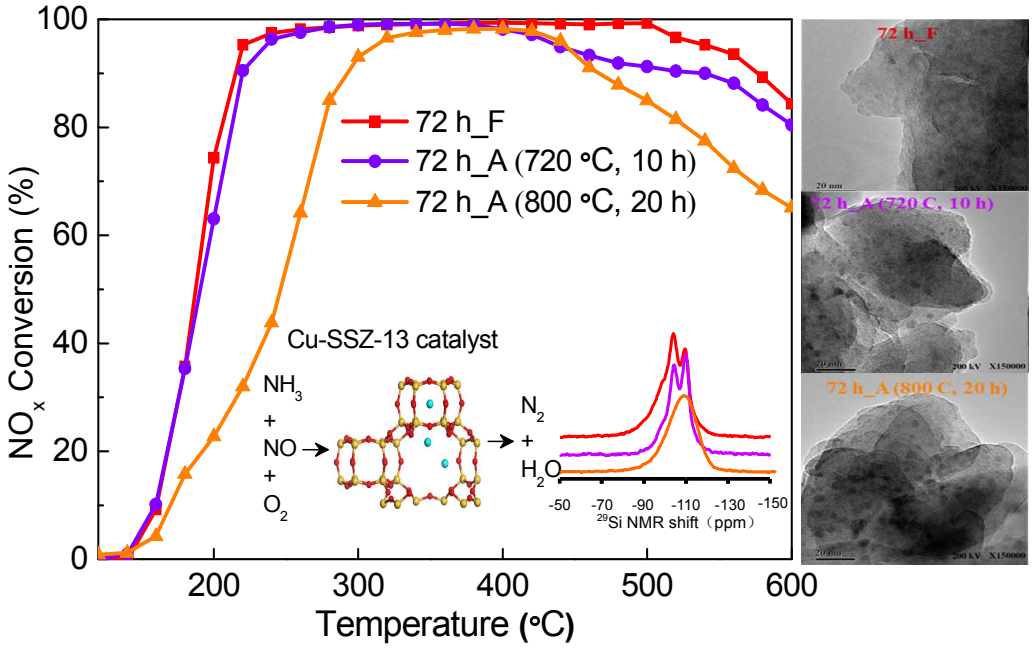

Influence of aging on in-situ hydrothermally synthesized Cu-SSZ-13 catalyst for NH_3-SCR reaction

Jiancheng Wang[a], Zhaoliang Peng[a], Hui Qiao[a], Lina Han[a], Weiren Bao[*a], Liping Chang[a], Gang Feng[*b], Wei Liu[*b]

[a.] *State Key Laboratory Breeding Base of Coal Science and Technology Co-founded by Ministry of Science and Technology and Shanxi Province, Taiyuan University of Technology, Taiyuan 030024, China*

[b.] *Shanghai Research Institute of Petrochemical Technology SINOPEC, Shanghai 201208, P.R. China*

**Corresponding author. E-mail address: baoweiren@tyut.edu.cn* (W. Bao)*; fengg.sshy@sinopec.com* (G. Feng); *liuw.sshy@sinopec.com* (W. Liu)

Abstract: Selective catalytic reduction (SCR) of NO_x by ammonia in the presence of excess oxygen becomes a potential method to remove NO_x from diesel exhaust. The present work optimized the Si/Al ratios and crystallization time for the in-situ hydrothermal synthesis of Cu-SSZ-13, which is a high efficient catalyst for SCR. The NH_3-SCR activities of the fresh and aging Cu-SSZ-13 samples were evaluated using a fixed bed reactor. The Cu-SSZ-13 crystallized 72 h showed better catalytic activity and hydrothermal stability than other catalysts. The fresh samples presented excellent $DeNO_x$ catalytic activities even under large space velocity (640,000 h^{-1}). Preliminary aging treatment (720 ^oC, 10 h) had slight negative effects on the SCR activity of the samples. Deep aging treatments (800 ^oC, 20 h) deactivated the catalyst significantly. The TEM, XRD, NMR, EPR, H_2-TPR, XPS and N_2 adsorption were carried out to elucidate the deactivation mechanism of the aging SCR catalyst. It was found that deep aging treatments resulted in the severe dealumination, the damage of the zeolite framework and the change of active copper species of the catalyst, which finally led to the poor catalytic activity of NH_3-SCR.

Key words: Cu-SSZ-13, Si/Al ratio, in-situ hydrothermal synthesis, crystallization time, hydrothermal aging, SCR-NH_3.

1. Introduction

Diesel engines offer several advantages, such as high power, better fuel economy and less CO and hydrocarbons (HCs) products, which has been paid much attention.[1] However, they issue much more nitrogen oxides (NO_x), which largely contribute to the formation of photochemical smog, ozone depletion and acid rain.[2] Nowadays, the reduction of NO_x from diesel engines remains a challenge because traditional three-way catalysts do not work well in lean combustion processes condition.[3] Thus, selective catalytic reduction (SCR) of NO_x by ammonia in the presence of excess oxygen becomes a potential method to remove NO_x from diesel exhausts.[4-6] Among the various catalysts developed for NH_3-SCR, zeolite-supported base metal (e.g. Cu, Fe) catalysts are currently being used in SCR after-treatment converters for meeting the diesel NO_x emission.[7,8] Iron-based zeolite catalysts, e.g., Fe-ZSM-5 and Fe-Beta,[9,10] have been considered to be efficient SCR catalysts at higher temperatures (> 300 ^{o}C), while its activity are significantly lower than the Cu catalysts in the low temperature range. Similarly, the significant research effects have been paid to the Cu^{2+} ion-exchanged ZSM-5 (Cu-ZSM-5) zeolites to illuminate both its NO_x decomposition and SCR activities.[11] However, it was found that Cu-ZSM-5 deactivates readily during high-temperature filter regeneration.[7]

Recently, SCR catalyst formulations containing Cu/zeolites with the chabazite (CHA) structure, such as Cu-SSZ-13 and Cu-SAPO-34, were successfully developed for diesel vehicles application.[12-19] SSZ-13 and SAPO-34 are the typical representative of zeolite with CHA structure, which contain small radius (~3.8 Å) eight-membered ring pores composed of six-membered rings, and such structure contributes to promising hydrothermal stability.[12] Until now, extensive studies have been carried out for Cu-SSZ-13 prepared via ion-exchange. The results indicated that Cu^{2+} ion-exchanged SSZ-13 (Cu-SSZ-13) was more active and shown better selectivity in the reduction of NO_x with NH_3 compared to other Cu/zeolites catalysts (e.g. Cu-ZSM-5, Cu-Beta).[13, 15, 20] Cu-SSZ-13 was considered to be one of the most promising candidates for practical application in NO_x removing

from diesel exhaust. However, the template used for the synthesis of SSZ-13, N,N,N-trimethyl-1-adamantammonium hydroxide (TMAdaOH) [21, 22] is so expensive that the wide application of SSZ-13 in industry is limited. Recently, a low-cost and novel template, copper-tetraethylenepentamine (Cu-TEPA), was found by Ren *et al*. for Cu-SSZ-13 synthesis via in-site hydrothermal synthesis method,[23, 24] which is more convenient compared with ion-exchange method. However, the influence of aging on the in-situ hydrothermally synthesized Cu-SSZ-13 are still not well investigated, which is important to understand the origin of high activity and the cause of activity decline after aging treatment of Cu-SSZ-13.

In this paper, the Cu-SSZ-13 catalysts were prepared via in-site hydrothermal synthesis method using copper-tetraethylenepentamine (Cu-TEPA) as template. The crystallization time and Si/Al ratio were optimized. The aging treatments of the catalysts were carried using a gas flow containing 10 vol% H_2O at 700~800 ^oC. The X-ray diffraction (XRD), transmission electron microscope (TEM), hydrogen temperature programmed reduction (H_2-TPR), nuclear magnetic resonance (NMR), inductively coupled plasma-auger electron spectroscopy (ICP-AES), N_2 adsorption, X-ray photoelectron spectroscopy (XPS), and electron paramagnetic resonance (EPR) were carried out to elucidate the deactivation mechanism of the aging samples.

2. Experimental

2.1 Catalyst preparation

Cu-SSZ-13 with different Si/Al ratio was synthesized using copper complex (Cu-TEPA) as the template, and the procedures were as follows. The gel was prepared with the molar ratios of $2.5Na_2O:1.0Al_2O_3:(2,4,6,7,8)SiO_2:147.7H_2O:1.47$Cu-TEPA, then the gel was divided into different PTFE liners of 50 ml autoclave, sealed, the gel was statically crystallized for 72 h, the optimum Si/Al ratio was acquired. The gel with optimum Si/Al ratio was prepared, and crystallized for 48 h, 72 h, 96 h, and 120 h at 140 ^oC, respectively. The solid products were washed with deionized H_2O and dried at 100 ^oC in air for 12 h. The dried powder was ion exchanged with NH_4NO_3 solution (1 mol/L)

for 12 h at 80 ^{o}C, then the zeolites was dried in air and calcined at 550 ^{o}C for 8 h.

2.2 Catalyst activity tests

Catalytic activities of the prepared samples were evaluated with a fixed-bed flow microreactor. First, the catalysts were tableted, ground and sieved to 0.25~0.43 mm before evaluation. Catalysts powder (0.15 ml) was placed in a quartz tube (Φ=8.5 mm) with silica wool, which was then placed inside an electric furnace. Before testing, the reactor was swept by helium gas at a flow rate of 100 ml/min to replace the air, and then the feed gas was switched to reaction gas (0.5% NO, 0.5% NH_3, 5% O_2, and He as balance, a total flow rate of 100 ml/min) for 30 min, the gas hourly space velocity (GHSV) were 40,000~640,000 h^{-1}. The NO_x-SCR activities of Cu-SSZ-13 were investigated in the temperature range of 100~600 ^{o}C with a heating rate of 8 ^{o}C/min. The simulated exhaust gas were analyzed simultaneously on-line by flue gas analyzer (British, Kane-9106), the NO conversion was calculated based on the following equation:

$$X = (c_1 - c_0)/c_1 \times 100\%,$$

Where, X is the conversion of NO_x, c_1 and c_0 are the concentration of NO_x before and after the reaction, respectively.

Catalyst selectivity was measured under the same experimental conditions, with the outlet gas analyzed through an on-line gas chromatograph (GC-9890A, Linghua Instrument Co., Ltd., Shanghai, China) equipped with a Porapak Q column for detection of N_2O.

In order to investigate the effects of hydrothermal treatment on the prepared samples, some of the catalysts (with the optimum Si/Al ratio and different crystallized time) were further treated in Ar gas flow, which contained 10 vol% vapor, at 720 ^{o}C for 10 h (preliminary aging) and at 800 ^{o}C for 20 h (deep aging).

2.3 Catalyst characterization

X-ray diffraction (XRD) measurements were carried out on a Rigaku D/MAX2500 instrument with Cu Kα radiation source (λ = 0.154056 nm), a tube voltage of 40 kV and a tube current of 100 mA.

The scanning rate was 8°/min within the 2θ value of 5~60°.

SEM pictures of the samples were obtained by JEOL Jsm-6700F field emission scanning electron microscope with an accelerating voltage of 10 kV. The samples were sprayed with gold prior to measurements.

TEM images were gained using a JEM-2010 transmission electron microscope with an accelerating voltage of 200 kV. The method of sample preparation for TEM measurement is as follows, the catalysts were ground and suspended in ethanol, dispersed over a carbon-coated holey Cu grid with a film.

Hydrogen temperature-programmed reduction (H_2-TPR) experiments were conducted with a PX200A equipment developed by Tianjin Pengxiang corporation, in which 60 mg of sample was loaded into a quartz reactor and pretreated at 120 ^{o}C for 2 h in Ar atmosphere. After cooling to room temperature, the gas was switched to the reducing gas (10% H_2/Ar, 50 ml/min) and the reduction test was performed from room temperature to 650 ^{o}C with a rate of 10 ^{o}C/min.

Solid state NMR spectra were obtained at room temperature on a Varian 400 spectrometer, 4 mm ZrO_2 rotors with a spinning rate of 10 kHz. ^{27}Al MAS NMR spectra were recorded at a resonance frequency of 104.26 MHz. ^{27}Al chemical shifts were reported relative to 0.1 M aqueous $Al(NO_3)_3$ solution. ^{29}Si MAS NMR measurements were performed at a resonance frequency of 79.49 MHz. The ppm scale was referenced to $Si(CH_3)_4$.

The Cu contents of the samples were analyzed by the inductively coupled plasma-auger electron spectroscopy (ICP-AES, Atomcan-16, America).

The pore structure properties of the samples were measured using a JW-BK122W N_2 adsorption instrument (JWGB Sci. & Tech. Co., Ltd., Beijing) at –196 ^{o}C. Microspore volume and diameter were calculated with HK method according to the sorption isotherm, the diameter was the most probable aperture.

X-ray photoelectron spectroscopy (XPS) surface analysis was conducted to determine the Cu

concentration on the surface as well as the binding energy of Cu 2p in the catalysts. The spectra were acquired with an AXIS ULTRA DLD spectrometer (Shimadzu Kratos Ltd., JPN) equipped with an Al Kα radiation source ($h\nu$ = 1486.6 eV).

The EPR spectra were obtained using a Bruker EMX spectrometer (USA) at 293 K (room temperature) and 155 K. The Bruker BioSpin WinEPR spectrometer software was used for data analysis. Spectra were recorded at both ambient (~293 K) and 155 K temperatures. For measurement, powder samples (~50 mg) were placed into quartz tubes and sealed with a plastic cover.

3. Results and discussion

3.1 Catalyst activity and selectivity

Fig. 1 shows the variation of $DeNO_x$ catalytic activities of Cu-SSZ-13 samples with different Si/Al ratios (a), different crystallization time samples before (b) and after (c) aging treatment, and different GHSVs as the temperature rises. As shown in Fig 1a, the active temperature windows become broader as the Si/Al ratio increases from 4 to 14. While, the active temperature window of the sample with the Si/Al ratio of 16 is much narrower than those of the others samples. Thus, combined with the XRD results in Fig 3 (see details below), it could be judged that the Si/Al ratio of 14 is optimum.

(Fig. 1)

The samples with different crystallization under the condition of Si/Al ratio = 14 were chosen for catalytic activity test and characterization.

As shown in Fig 1b, NO_x reduction activities of fresh samples increased as the temperature rises, reaching 90~100% conversion at 220 ^{o}C. In addition, the high NO_x reduction efficiencies (90~100%) of fresh samples crystallized for 72 h, 96 h, and 120 h could be sustained to 560 ^{o}C. The efficiency of the fresh sample crystallized for 48 h could only be sustained to 520 ^{o}C. Further increase the temperature to 600 ^{o}C, the NO_x conversions were maintained above 80% over fresh samples crystallized for 72 h, 96 h, and 120 h, respectively, v.s. 60% for the fresh sample crystallized for 48 h. The $DeNO_x$ catalytic activities of samples are better than the reported data in ref. 8, 17, which are

above 80% ($DeNO_x$ efficiencies) in 250~500 ^oC. Fig. 1c indicates that the NO_x catalytic activities of preliminary aging (720 ^oC aged 10 h) samples reached 90%~100% in the temperature range of 240~500 ^oC. There is no obvious difference for the catalytic activities of preliminary aging samples with different crystallization time. In order to further investigate the effects of hydrothermal aging treatment for the structure and the performance of Cu-SSZ-13, the fresh samples crystallized for 72 h and 96 h were also treated with aging conditions at 800 ^oC for 20 h. Compared with the fresh samples (Fig 1a and 1b), it shows that the hydrothermal aging treatment had some negative effects on the catalyst activities (Fig 1c), the activity temperature window became narrower. Although the temperature window of high activity (above 90%) became to 300~460 ^oC, the NO_x conversion rates were still above 60% at high temperatures (> 600 ^oC). In addition, the sample crystallized for 72 h showed better thermal stability than other samples. It was also found that deep aging treatment deactivates the catalyst more severely than preliminary aging treatment.

Fig. 1d shows the NO_x conversions of the SCR of NO_x with ammonia under different GHSVs over the Cu-SSZ-13 sample crystallized in 72 h. It shows that the NO_x conversions of NH_3-SCR decreased as the GHSV increases from 40,000 to 640,000 h^{-1}, especially for the temperature below 250 ^oC. This trend became inconspicuous above 500 ^oC. It should be noted that the Cu-SSZ-13 sample displayed high NO_x conversions beyond 80% within a broad temperature window of 300~550 ^oC even under a very high GHSV of 640,000 h^{-1}. The catalyst performed satisfactorily resistance to the effects of large space velocity comparing to other catalysts which displayed the NO_x conversions over 80% under GHSV of 100,000 h^{-1} within a temperature window from 300 to 450 ^oC.[25] This would enable the catalyst to achieve practical application in diesel vehicles with limited installation space.

(Fig. 2)

The N_2O selectivity is another important parameter, except the NO_x conversion, for the evaluation of the NH_3-SCR catalysts performance. The traces of N_2O formation over Cu-SSZ-13 samples with

different crystallization time before and after hydrothermal aging treatment were shown in Fig. 2. It was observed that the outgas N_2O concentrations of the fresh samples with different crystallization time are less 10 ppm. The maximum amount of N_2O was produced at 300 ^oC. Fig 2b demonstrates that the N_2O yields of hydrothermal aging samples increased to some extent, especially for the temperature range of 300~500 ^oC, while less than 15 ppm. It should be pointed out that the conversion rate of NO_x transforming to the innoxious N_2 was still higher than 94%. This result is consistent with the reported results in ref. 8, 26. The N_2O yields of aging samples increase in high temperature regions probably related to the special copper species (Cu-AlO_x) transformed or migrated from the isolated Cu^{2+} species.[8, 27, 28]

3.2 Catalyst characterization

3.2.1 Structural properties

In order to investigate the optimal Si/Al ratio, crystallization time and the effects of hydrothermal aging on Cu-SSZ-13 catalysts, the crystal structure of different Cu-SSZ-13 catalysts were characterized using XRD, and the results are displayed in Fig. 3. Fig 3a displays the XRD profiles of samples with different Si/Al ratios. It shows that the characteristic peaks of SSZ-13 at 2θ = 9.5°, 14.0°, 16.1°, 17.8°, 20.7°, 25.0°, and 30.7° were observed for the samples with Si/Al ratios less than 14. The peak intensity increases as Si/Al ratio increases. While for the sample with Si/Al ratio of 16, the diffraction peak of SSZ-13 could hardly be checked. These results are in well consistent with variation of $DeNO_x$ catalytic activities, i.e. the $DeNO_x$ catalytic activities of the samples increases as the Si/Al ratios increases when the Si/Al ratio were less than 14. While the sample with Si/Al of 16 showed poor $DeNO_x$ catalytic performances.

(Fig. 3)

As shown in Fig 3b and 3c, the characteristic peaks of SSZ-13 were observed in both the fresh and preliminary aging samples with different crystallization time. Fig. 3b shows that all the fresh samples have high crystallinity. Furthermore, the diffraction peaks of samples crystallized for 48 h and 72 h

are weaker than that of samples crystallized for 96 h and 120 h to some extent. The phenomenon indicates that prolonging the crystallization time has a positive role on the enhancing crystallinity of the samples. Fig. 3c demonstrates that the intensity of diffraction peaks in preliminary aging samples decreases slightly. Moreover, the peaks intensity of the preliminary aging sample crystallized for 72 h are higher than other aging samples, it indicates that the peaks intensity of the sample crystallized for 72 h reduces less than other samples after the aging treatment. It is interesting to note that no diffraction peaks of copper species are found in the XRD patterns of all samples. This is probably due to different types of copper species formed on the Cu-SSZ-13 catalyst (details will be discussed in the H_2-TPR part). While it could be deduced that no matter which type of copper exists in the Cu-SSZ-13 samples, copper species are highly dispersed in the samples.[7, 20, 29] Thus, the diffraction peak of copper species could not be observed in the XRD patterns of all samples. For the deep aging samples, diffraction peak of SSZ-13 almost disappeared, demonstrating the deep aging treatment seriously destroyed the crystalline structure of the zeolites.

(Fig. 4)

The sample crystallized for 72 h was characterized using transmission electron microscopy (TEM) and the results are shown in Fig. 4. It shows that the crystalline and morphology of the sample were seriously damaged, as the aging treatment became more severe. No visible particles are seen in the fresh sample, indicating that the Cu species are highly dispersed. For the sample aged at 800 ^{o}C for 20 h, XRD pattern (shown in Fig. 3.) indicated a complete lack of zeolite structure, TEM image demonstrates that some black particles appeared in the aging sample and the amount of black particle increases as the aging degree increases. The black particles could be some special copper species (maybe CuO clusters) resulted from isolated Cu^{2+} migration or transformation. Thus, it could be deduced from the TEM results that the hydrothermal aging treatment destroyed the crystalline and morphology of the Cu-SSZ-13 sample and the active copper component maybe changed during the hydrothermal aging treatment.

3.2.2 H_2-TPR

H_2-TPR experiments were carried out to examine the species of the copper in the fresh and aging Cu-SSZ-13 samples, and the results are shown in Fig. 5. As shown in Fig. 5a, fresh samples with different crystallization time showed four hydrogen reduction peaks located at 180, 220, 275, and 500 ^{o}C. It is well known that there are four types of cationic sites in CHA.[30, 31] The previous works of Fickel and Lobo proposed that copper ions are located only in six-membered ring windows of SSZ-13.[20] While, Kwak et al. hypothesized that there are two types of copper species formed on the Cu-SSZ-13, the first copper ions occupy sites in the six-membered rings, the second copper ions occupy sites inside the large cages of the CHA structure.[7] In this study, not only was copper the main active material, but also used for copper-tetraethylenepentamine (Cu-TEPA) as template. After calcinations, the TEPA was removed, copper ions stayed in the framework or surface structure, which indicates that copper ions occupied in different positions thus leading to diverse catalytic activities at different temperature. In our H_2-TPR results, the peaks of 180 ^{o}C, 220 ^{o}C and 275 ^{o}C were assigned to the reduction of Cu^{2+} to Cu^{+}. The H_2-TPR peaks at 180 ^{o}C are due to reduction of isolated Cu^{2+} ions located near the eight-membered ring window. The peaks at 220 ^{o}C are attributed to reduction of isolated Cu^{2+} ions located in different O atoms of the large cages of the CHA structure. The peaks at 275 ^{o}C are ascribed to reduction of isolated Cu^{2+} ions located in six-membered ring. The multitudinous copper ions which are easily reduced maybe lead to the excellent activity of fresh samples.[32] Furthermore, the H_2-TPR peak of sample crystallized 48 h at 275 ^{o}C is weaker than that of other samples, probably because the crystallization time is too short to enable Cu^{2+} to occupy the sites of six-membered ring after saturation of sites inside the large cages of the CHA structure. Therefore, we conclude that after saturation of sites inside the large cages of the CHA structure, Cu^{2+} ions can then occupy the sites of six-membered ring. The broader reduction peak at 500 ^{o}C can be assigned to the reduction of Cu^{+} to Cu.

(Fig. 5)

Fig. 5b presents the H_2-TPR results of aging samples. For the preliminary aging samples, the hydrogen reduction peaks at 220 ^oC became narrower compared with the fresh samples in Fig. 5a. It indicates that the Cu^{2+} ions in the aging samples are in a more confined chemical environment than in the fresh samples. The disappearance of peak at 275 ^oC maybe because to the decrease for the amount of Cu^{2+} in aging sample. It should be noted that hydrogen reduction peaks at 375 ^oC were observed for the samples crystallized in 48 h and 72 h, and hydrogen reduction peaks at 320 ^oC on the samples crystallized 96 h and 120 h. These results can be explained by the reduction of some special copper species transformed or migrated from isolated Cu^{2+},[8, 27, 28] which may lead to the decline of catalytic activity. While for the deep aging (800 ^oC, 20 h) samples crystallized for 72 h and 96 h, there are two hydrogen reduction peaks at 220 ^oC and 320 ^oC, respectively. The peaks at 220 ^oC are weaker and narrower, while it is broader at 320 ^oC than that of preliminary aging samples. Similarly, this phenomenon could also be attributed to the transformation or migration of isolated Cu^{2+} to new complexes (such as Cu-AlO_x). The transformation or migration of isolated Cu^{2+} should be one of the main factors which lead to the decline of catalytic activity of the catalysts.

3.2.3 NMR

In order to investigate the effects of aging treatment on Si atoms and Al atoms in framework of Cu-SSZ-13, the samples crystallized 72 h and 96 h before and after aging treatment were characterized using solid state nuclear magnetic resonance (NMR). Fig. 6a and Fig. 6c show the ^{29}Si NMR spectra. The ^{29}Si NMR spectra of samples crystallized for 72 h and 96 h before and after preliminary aging treatment show two peaks at chemical shift of –101 ppm and –110 ppm, which are induced by the Si(2Al) and Si(0Al) coordination structure of the SSZ-13 zeolites, respectively.[33, 34] This phenomenon explains that preliminary aging treatment did not cause great damage to the framework of samples. It should be pointed out that, the peaks at –110 ppm is lower than the peaks at –101 ppm for the fresh samples, while it is higher than the peaks at –101 ppm for the preliminary aging samples. This is probably because that dealuminization occurred during the preliminary aging

treatment. Integrity of zeolite framework also plays an important role on keeping catalytic activity of catalysts. However, the peak of deep aging sample is almost impossible to distinguish, indicating that ordered framework structure of sample was damaged severely. The active center loses the support since the zeolite framework was damaged, and finally results in the catalysts deactivation.

(Fig. 6)

As shown in Fig. 6b and Fig. 6d, the ^{27}Al NMR spectra show one resonance peak at chemical shift of 58 ppm for samples crystallized 72 h and 96 h before and after preliminary aging treatment, which was ascribed to the tetrahedral coordination of alumina in the zeolite framework.[8, 35] In addition, the peak at chemical shift of 58 ppm becomes smaller after preliminary aging, which indicates that the dealuminization of the zeolites during the preliminary aging treatment occurs. This result agrees well with the ^{29}Si NMR spectra of the fresh and preliminary aging samples. For the deep aging samples, the relative intensity of resonance peak at chemical shift of 58 ppm decreased seriously, which was estimated about 50%. An additional peak appears around 0 ppm, which should be related to extra-framework octahedral coordination of alumina,[35] signifying that tetrahedral aluminum in the zeolite framework are changed to octahedral aluminum upon dealumination under the further aging treatment.[8] These results indicate that there exist the severe dealuminization and damage of the zeolite framework during the deep aging treatment. However, no new peaks associated with octahedral aluminum were observed in any of the samples. The lack of octahedral aluminum ions in the aged catalysts suggests that paramagnetic Cu ions may interact more strongly with the forming octahedral aluminum than zeolitic Cu ions with framework aluminum. It was possible that Cu and Al had agglomeration or reaction into the formation of special copper species (Cu-AlO_x) in severe conditions. In summary, the explanations of ^{27}Al NMR spectra are in well accordance with ^{29}Si NMR spectra. In addition, no obvious differences were found for the NMR results of samples crystallized

for 72 h and 96 h, this is also in accordance with the XRD characterization. Furthermore, the H_2-TPR results described above also indicate the transformation or migration of isolated Cu^{2+} to new complexes (Cu-AlO_x). This new complexes are derived from interaction of Cu and the dealuminated Al ions from the zeolite framework.[8] Thus, it could be deduced that the dealuminization and the transformation or migration of isolated Cu^{2+} concurred in the aging treatment, which contributes to the deactivation of the catalyst.

3.2.4 ICP

The Cu content in the Cu-SSZ-13 samples are shown in Table 1. For the fresh samples, the Cu content increased from 3.47 to 6.86% as the cryatallization time increased from 48 h to 120 h, which is in the same trend as the $DeNO_x$ catalytic activity of samples. The copper content reduced to less than 0.88% for the preliminary aging samples, v.s. about 2.8% for the deep aging samples with the cryatallization time of 72 h. The loss of total copper content can be ignored in consideration of the error of the ICP measurement. It indicates that the aging treatment mainly changed the forms of the copper species and further damaged the catalytic activity.

(Table 1)

3.2.5 N_2 adsorption

The pore-structure parameters of the Cu-SSZ-13 crystallized for 72 h and 96 h before and after aging treatment are summarized in Table 1.After preliminary aging treatment, the surface area of samples crystallized 72 h and 96 h slightly decreased (from 299 and 292 m^2/g to 256 and 256 m^2/g, respectively) by 14% and 12%, respectively. The pore volumes of the samples changed only a little before and after preliminary aging. Pore diameter increased (from 0.57 and 0.59 nm to 0.72 and 0.76 nm, respectively) by 26% and 29%, respectively, after preliminary aging. It indicates that the

preliminary aging treatment only results in very slight dealumination and damage of the zeolite framework. The pore volumes and surface areas decreased drastically by 15% and 31% (crystallized for 72 h), 10% and 30% (crystallized for 96 h), respectively, for the deep aging samples compare with the fresh samples crystallized for 72 h and 96 h. It is therefore assumed that the serious damage occurred to the framework of samples during the deep aging treatments.

3.2.6 XPS

Cu 2p XPS spectra of Cu-SSZ-13 samples crystallized 72 h before and after aging treatment are shown in Fig. 7. The samples present the main peak at 934.3 eV (with a slight shoulder around 935.2 eV) for Cu $2p_{3/2}$ and the transition peak at 952.8 eV for Cu $2p_{1/2}$, as well as the shake-up peaks at 942.5eV and 962.9 eV, which can be used as the characteristic peak of Cu^{2+}.[36-38] No obvious differences were found for the fresh and preliminary aging samples for the peak at 934.3eV, which indicates preliminary aging treatment has no much influence on the Cu species of the zeolite surface. While, the shake-up satellites decrease to some extent, implying the amount of Cu^{2+} decreased after aging treatment.[39] Meanwhile, for the further aging sample, the main transition peak dramatically decreased in intensity, because some Cu^{2+} transformed or migrated to other copper species and led to lower copper concentration on the surface (Table 2). In order to determine the valence of Cu element accurately, it is essential to refer to the auger parameters of different species. Generally, the distinction was made by using amendatory auger parameters a′ ($a' = E_k(CuL_3VV) + E_b(Cu\ 2p_{3/2})$) and the results are shown in Table 2. At the binding energy of 933.2 eV on the surface of the fresh and preliminary aging samples, Cu element, whose auger parameters a′ were respectively 1848.4 eV and 1848.2 eV, existed mainly in the form of Cu^{+}, and Cu^{2+}/Cu^{+} were severally 0.22 and 0.21. These results illustrate that, as for the existence state of Cu element on the samples' surface, there was not fundamental difference between the fresh sample and preliminary aging sample, which thereby led to little difference on catalytic activity. For deep aged samples, whose auger parameters a′ was 1848.5 eV, was located chiefly as Cu^{+}, and Cu^{2+}/Cu^{+} was 0.12. It indicates that deep aging treatment had

great effect on the formation of Cu species existing on the sample surface, resulting in the decrease of the Cu^{2+} proportion and damage on active metal Cu existence. Thus the deactivation of catalysts occurred.

(Fig. 7)

(Table 2)

The Cu surface concentrations, Si surface concentrations and Al surface concentrations are given in Table 2. Cu surface concentrations of the fresh, preliminary aging and deep aging samples are 0.31 wt%, 0.28 wt% and 0.25 wt%, respectively, v.s. the Al surface concentrations of 0.82 wt%, 1.08 wt% and 1.12 wt%. Si surface concentrations did not show obvious changes. This result indicates that the decrease of sample activity was caused by the migration and transformation of the catalyst active centers as well as the damage of the molecular sieve framework. In other words, isolated Cu^{2+} and Al species come from framework reacted and Cu-AlO_x species was formed.

3.2.7 EPR

Fig. 8 displays EPR results of the hydrated Cu-SSZ-13 samples before and after aging treatment measured at room temperature (a) and 155 K (b). As shown in Fig. 8a, two features presents at high field about 3334 and 3407 G. The feature at 3407 G became narrower after aging treatment. This change may indicate a slight decomposition of Cu-SSZ-13 sample during the aging treatment,[40] which leads to the decrease of Cu^{2+} amount. Thus, the catalytic activity of samples decreased to some extent. The hyperfine structure of isolated Cu^{2+} species can be characterized by EPR spectra. In order to reduce the Cu^{2+} ion mobility and allow only dipole–dipole interactions to be detected, EPR measurements at 155 K were performed. As shown in Fig. 8b, only a single spectral feature is detected, and the hyperfine structure of isolated Cu^{2+} species are better resolved in the low field. Moreover, by analyzing the hyperfine features, the EPR signals at $g_{\parallel} = 2.38$ with $A_{\parallel} = 136$ G (Cu^{2+}(a)), $g_{\parallel} = 2.35$ with $A_{\parallel} = 149$ G (Cu^{2+}(b)), and $g_{\parallel} = 2.33$ with $A_{\parallel} = 155$ G (Cu^{2+}(c)) are gained, which manifest three distinct Cu^{2+} species. Cu^{2+}(a) could be assigned to Cu^{2+}coordinated to three oxygen

atoms on the six-ring sites according to the previous reports;[28, 41] Cu^{2+}(b) could be assigned to isolated Cu^{2+} species located inside the large cages of the CHA structure: Cu^{2+}(c) could be assigned to isolated Cu^{2+} ions located near the eight-membered ring window.[32] The results of EPR are in accordance with the aforementioned H_2-TPR analysis. It should be also noted that the intensity in the EPR spectra decreased as the aging treatment became more severe, despite essentially unchanged in shapes, indicating the coordination environment of Cu^{2+} changed and the amounts of Cu^{2+} content decreased. These results agree well with the previous work that the transformation or migration of Cu^{2+} results in the deactivation of the catalysts.[28]

(Fig. 8)

4. Conclusions

The Si/Al ratios and crystallization time were optimized for the in-situ hydrothermal synthesis of the Cu-SSZ-13. NH_3-SCR activities of Cu-SSZ-13 samples were evaluated using a fixed bed reactor, and the effects of hydrothermal aging on the catalytic properties of the zeolites were investigated. The fresh samples showed excellent $DeNO_x$ catalytic activities even under large space velocity (640,000 h^{-1}). The Cu-SSZ-13 crystallized 72 h show better catalytic activity and hydrothermal stability than other catalysts due to its optimal crystallization structure and active component content. Preliminary aging treatment (720 ^oC, 10 h) had slight effects on the samples, and the $DeNO_x$ ability of Cu-SSZ-13 reduced a little compared to the fresh samples. However, deep aging treatment (800 ^oC, 20 h) showed a significant influence on the zeolites, since sever dealumination resulted in the damage of the zeolite framework and copper species also changed. The structure and active copper species of the zeolites changed for the deep aging samples, and led to the poor catalytic activity of NH_3-SCR. The conversion efficiencies of NH_3-SCR across the entire temperature window decreased for the deep aging samples. In addition, the N_2O selectivity of the aging samples decreased after aging treatment to some extent, especially in the high temperature region (400~500 ^oC), while the rate of NO transformed to the innoxious N_2 was still above 94%.

Acknowledgements

The authors gratefully thank the financial support from the Program for the Top Young Academic Leaders of Higher Learning Institutions of Shanxi, NSFC (20906067), and CPSF (2011M500543).

Table 1 Cu content and pore structure of Cu-SSZ-13 before and after aging treatment.

Sample	Cu_{bulk} (wt%)	A_{BET} (m^2/g)	V_t (cm^3/g)	D (nm)
48 h_F	3.47			
72 h_F	5.65	299	0.26	0.57
96 h_F	6.57	292	0.29	0.59
120 h_F	6.86			
72 h_A (720 ^{o}C, 10 h)	5.60	256	0.27	0.72
96 h_A (720 ^{o}C, 10 h)	6.54	256	0.29	0.76
72 h_A (800 ^{o}C, 20 h)	5.49	206	0.22	0.63
96 h_A (800 ^{o}C, 20 h)	6.46	204	0.26	0.65

Table 2 Cu and Si contents on the surface of Cu-SSZ-13 according to the XPS results.

Sample	Cu_{sur} (wt%)	E_b(Cu $2p_{3/2}$) (eV)	E_k(Cu L_3VV) (eV)	a'(Cu) (eV)	Cu^{2+}/Cu^{+}	Si_{sur} (wt%)	Al_{sur} (wt%)
72 h_F	0.31	933.2	915.2	1848.4	0.22	3.80	0.82
72 h_A (720 ^{o}C, 10 h)	0.28	933.2	915.0	1848.2	0.21	3.83	1.08
72 h_A (800 ^{o}C, 20 h)	0.25	933.1	915.4	1848.5	0.12	3.87	1.12

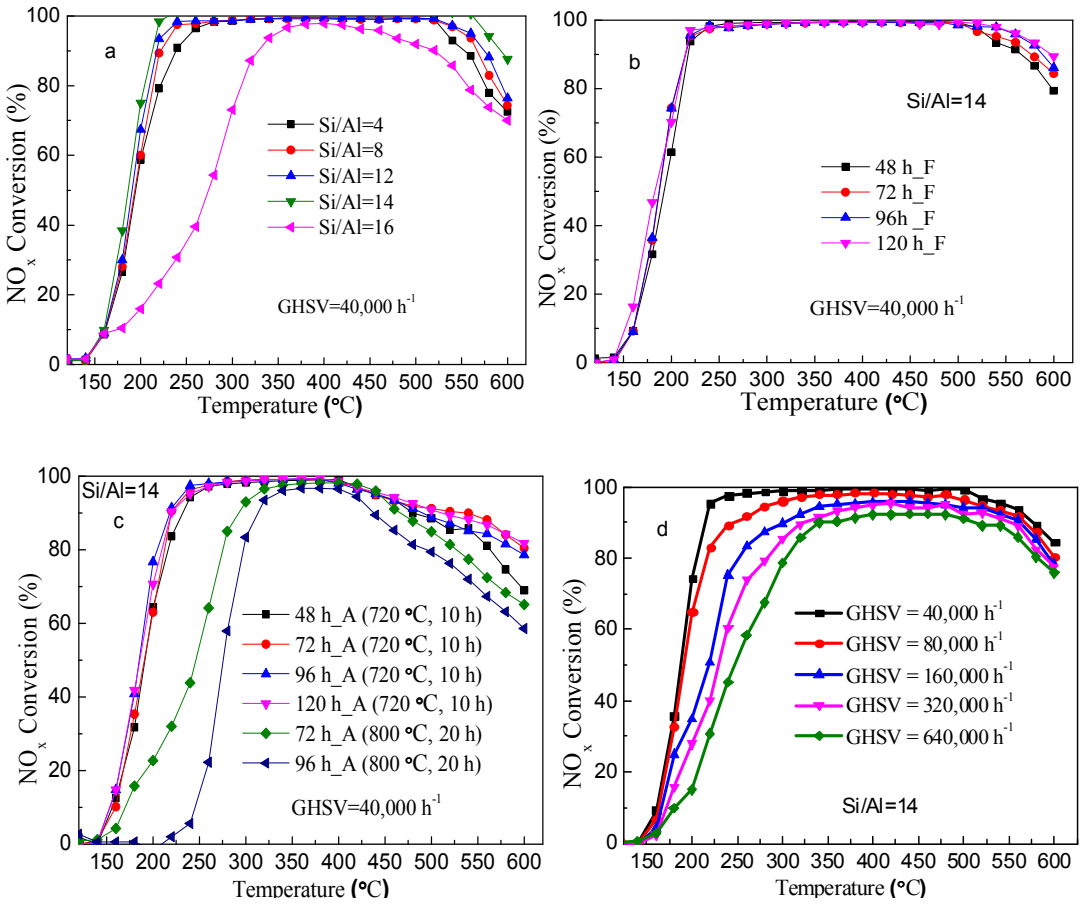

Fig. 1. Catalytic performance for SCR of NO_x with ammonia of Cu-SSZ-13 samples.

a: fresh samples with different Si/Al ratios; b: fresh samples with different crystallization time; c: aged samples with different crystallization time; d: under different GHSVs over Cu-SSZ-13 samples crystallized in 72 h. Reaction conditions: 500 ppm NO, 500 ppm NH_3, 5% O_2, balance He.

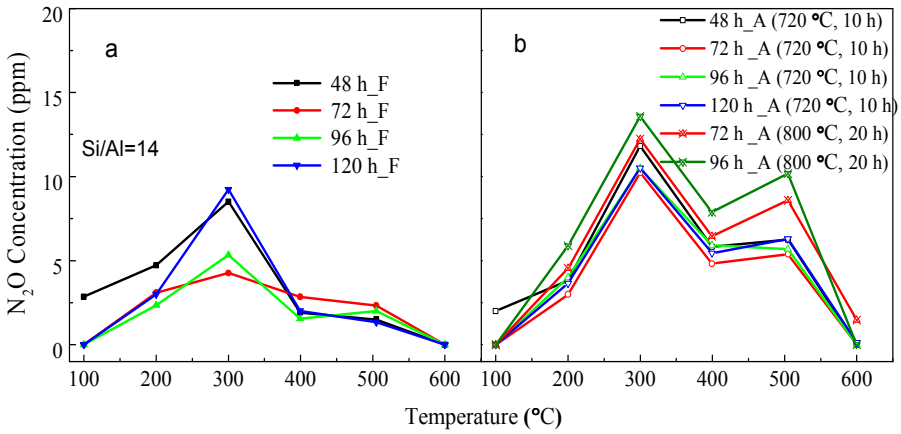

Fig. 2. N_2O concentration over Cu-SSZ-13 samples with different crystallization time before (a) and after (b) hydrothermal aging.

Reaction conditions: 500 ppm NO, 500 ppm NH_3, 5% O_2, balance He, and GHSV = 40,000 h^{-1}.

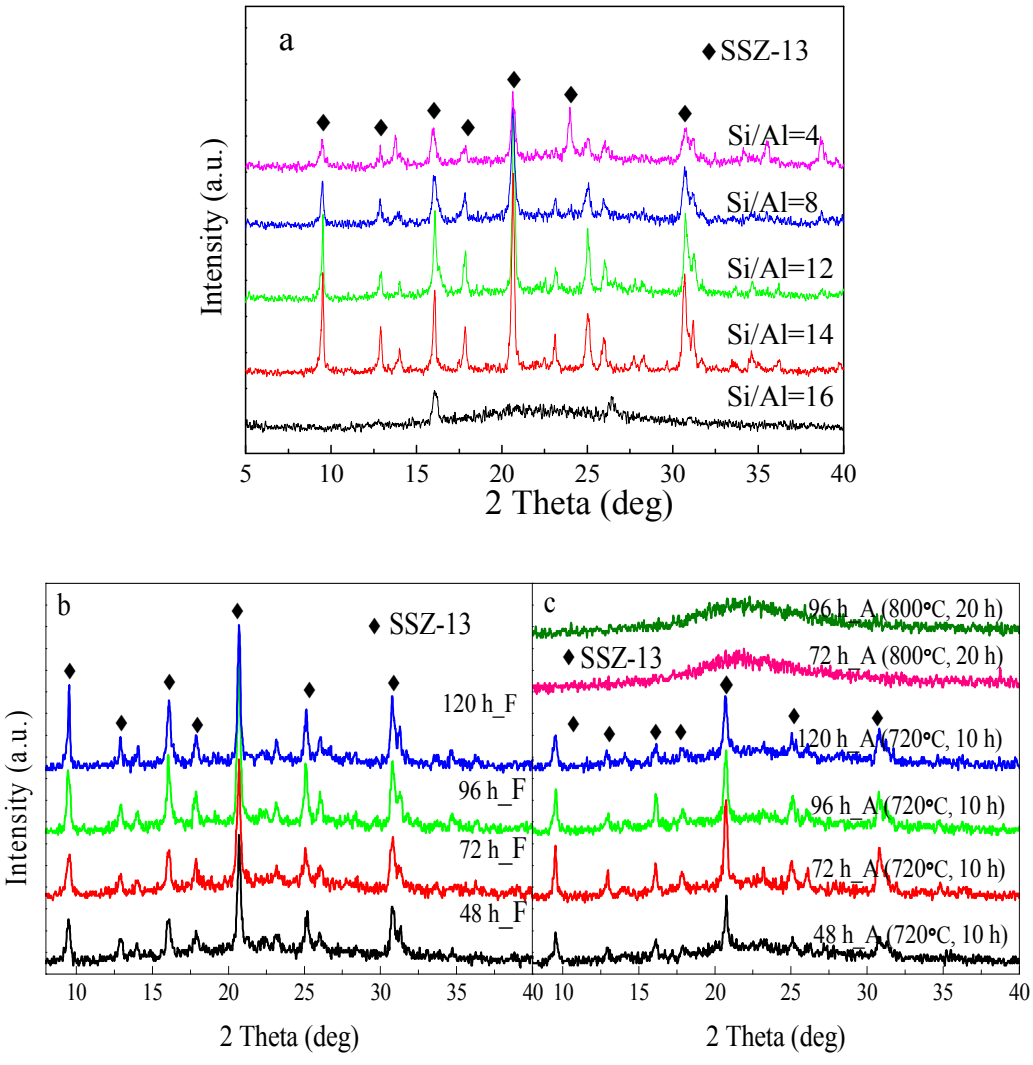

Fig. 3. XRD patterns of Cu-SSZ-13 samples.

a: fresh samples with different Si/Al ratios; b: fresh samples with different crystallization time; c: aged samples with different crystallization time.

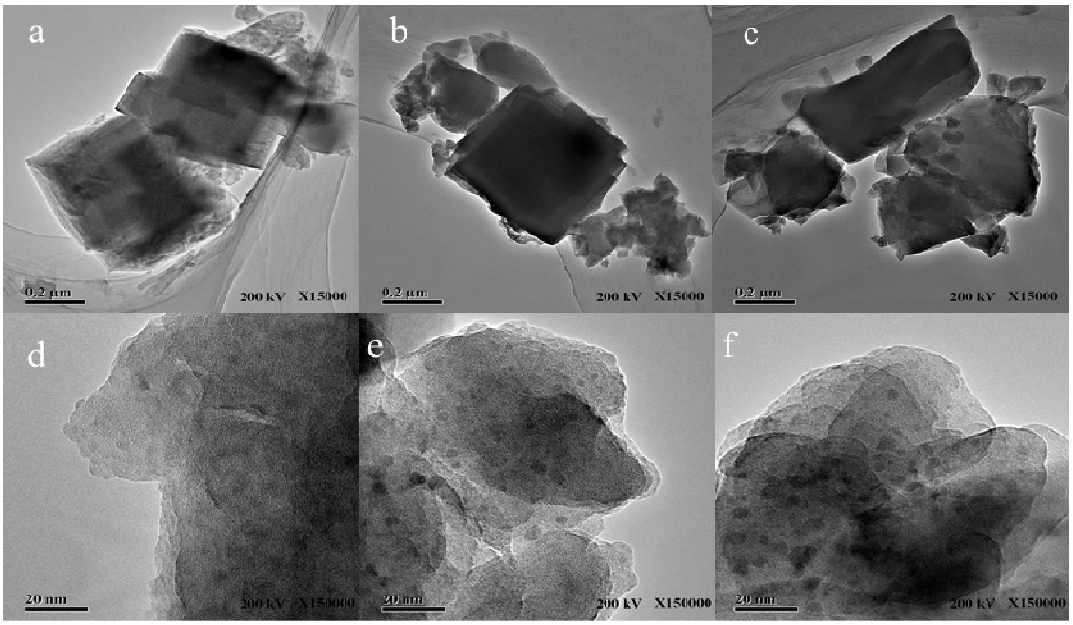

Fig. 4. TEM images of Cu-SSZ-13 crystallized for 72 h before and after aging.

a, d: 72 h_F; b, e: 72 h_A (720 ^{o}C, 10 h); c, f : 72 h_A (800 ^{o}C, 20 h).

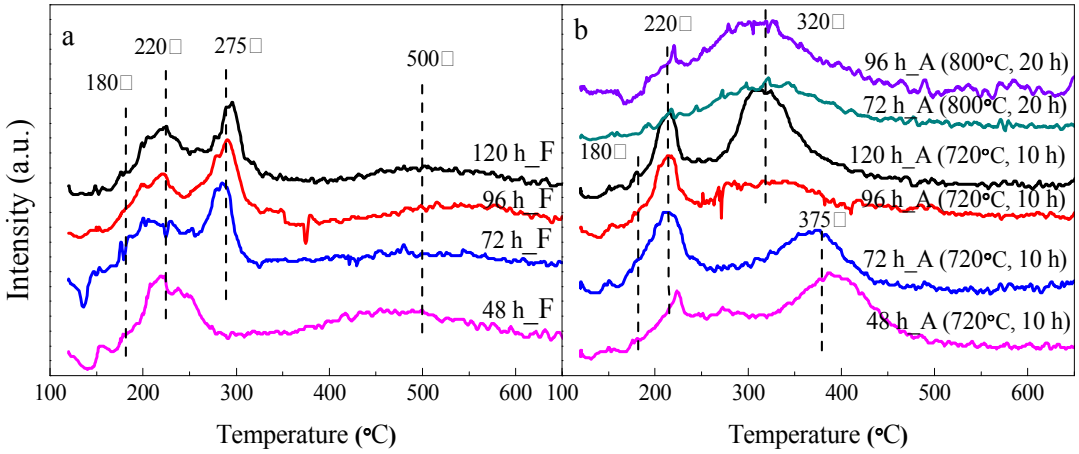

Fig. 5. H_2-TPR profiles of Cu-SSZ-13 samples with different crystallization time before (a) and after (b) aging

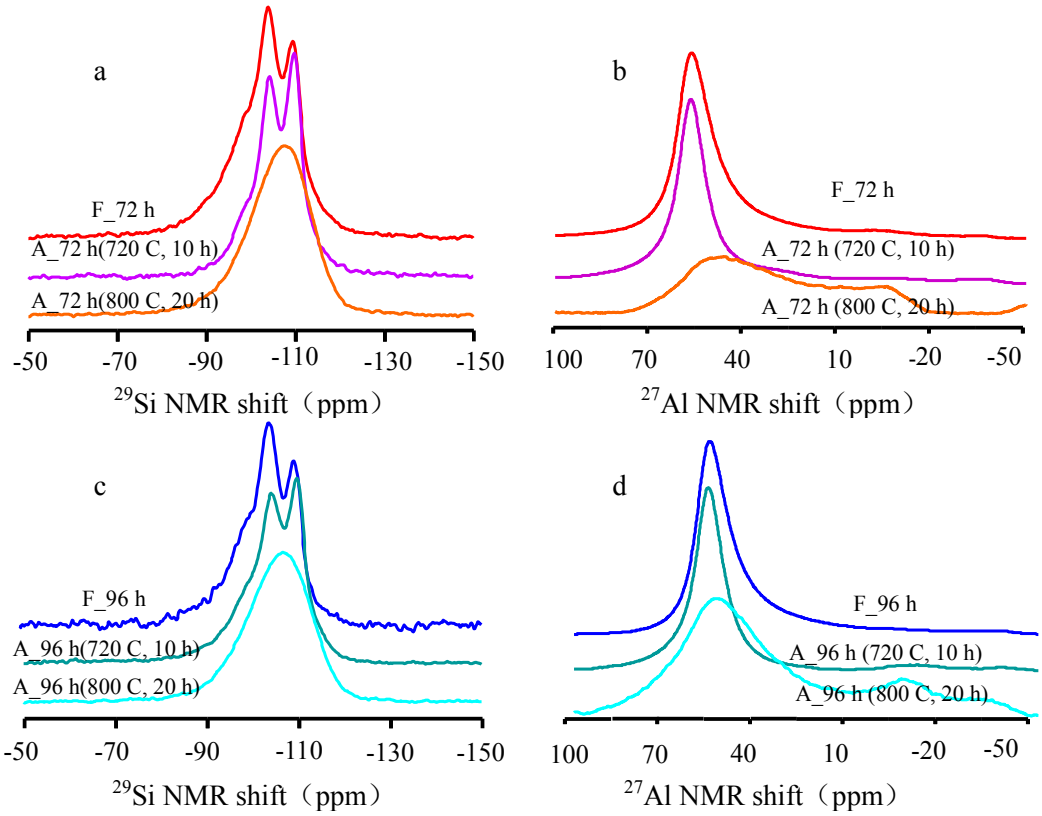

Fig. 6. Solid state ^{29}Si NMR and ^{27}Al NMR spectra of Cu-SSZ-13 before and after aging.

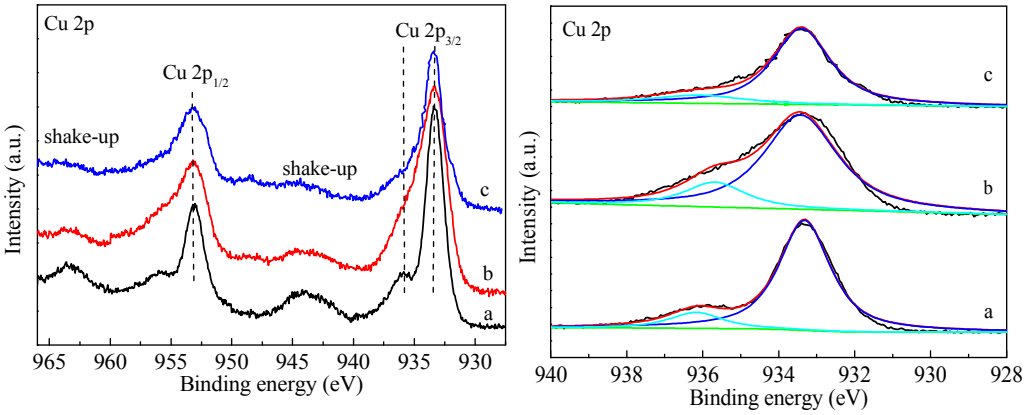

Fig. 7. Cu 2p XPS spectra of Cu-SSZ-13 samples before and after aging.

(a): 72 h_F; (b): 72 h_A (720 ^{o}C, 10 h); (c) 72 h_A (800 ^{o}C, 20 h).

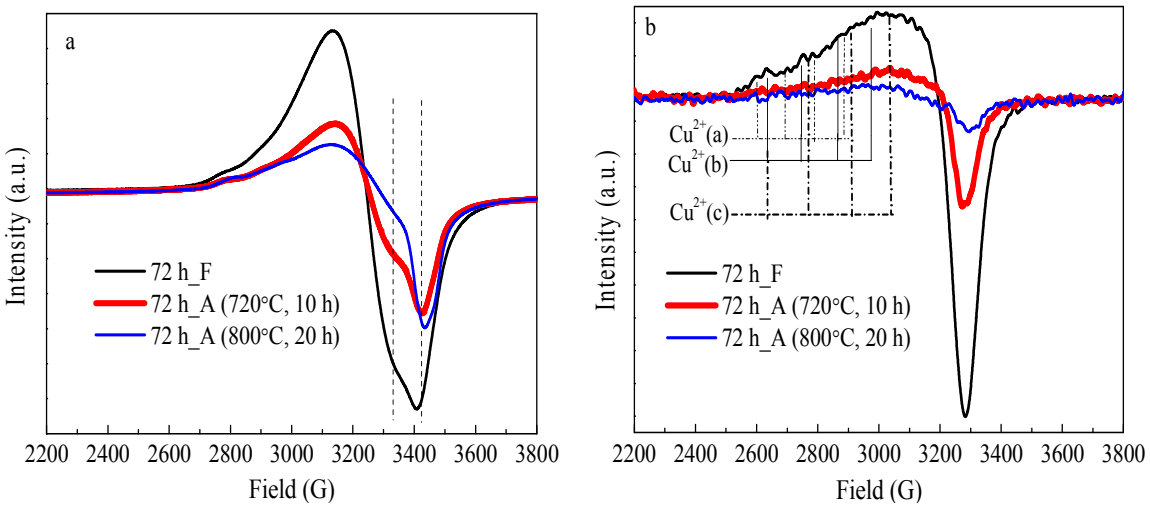

Fig. 8. EPR spectra of fresh and aged Cu-SSZ-13 samples measured at room temperature (a) and 155 K (b).

References

1 J. Kašpar, P. Fornasiero and N. Hickey, *Catal. Today*, 2003, **77**, 419-449.

2 A. Fritz and V. Pitchon, *Appl. Catal. B*, 1997, **13**, 1-25.

3 R. J. Farrauto and R. M. Heck, *Catal. Today*, 1999, **51**, 351-360.

4 G. Busca, L. Lietti, G. Ramis and F. Berti, *Appl. Catal. B*, 1998, **18**, 1-36.

5 G. Qi, R. T. Yang and R. Chang, *Appl. Catal. B,* 2004, **51**, 93-106.

6 D. Zhang, L. Zhang, C. Fang, R. Gao, Y. Qian, L. Shi and J. Zhang, *RSC Adv.*, 2013, **3**, 8811-8819.

7 J. H. Kwak, H. Y. Zhu, J. H. Lee, C. H. F. Peden and J. Szanyi, *Chem Commun (Camb).*, 2012, **48**, 4758-4760.

8 J. H. Kwak, D. Tran, S. D. Burton, J. Szanyi, J. H. Lee and C. H. F. Peden, *J. Catal.*, 2012, **287**, 203-209.

9 R. Q. Long and R. T. Yang, *Am. Chem. Soc.*, 1999, **121**, 5595-5596.

10 P. Balle, B. Geiger and S. Kureti, *Appl. Catal. B*, 2009, **85**, 109-119.

11 M. Iwamoto, H. Furukawa, Y. Mine, F. Uemura, S.-i. Mikuriya and S. Kagawa, *J. Am. Chem. Soc., Chem. Commun.*, 1986, 12723.

12 D. W. Fickel, E. D'Addio, J. A. Lauterbach and R. F. Lobo, *Appl. Catal. B*, 2011, **102**, 441-448.

13 J. H. Kwak, R. G. Tonkyn, D. H. Kim, J. Szanyi and C. H. F. Peden, *J. Catal.*, 2010, **275**, 187-190.

14 H. Tounsi, S. Djemal, C. Petitto and G. Delahay, *Appl. Catal. B*, 2011, **107**, 158-163.

15 J. H. Kwak, D. Tran, J. Szanyi, C. H. F. Peden and J. H. Lee, *Catal. Lett.*, 2012, **142**, 295-301.

16 J. S. McEwen, T. Anggara, W. F. Schneider, V. F. Kispersky, J. T. Miller, W. N. Delgass and F. H. Ribeiro, *Catal. Today*, 2012, **184**, 129-144.

17 L. Wang, W. Li, G. Qi and D. Weng, *J. Catal.*, 2012, **289**, 21-29.

18 J. C. Wang, H. Qiao, L. N. Han, Y. Q. Zuo, L. P. Chang, W. R. Bao and G. Feng, *J Nanomater.*, 2013, **2013**, 9.

19 Z. Q. Liu, L. Tang, L. P. Chang, J. C. Wang and W. R. Bao, *Chin. J. Catal.*, 2011, **32**, 546-554.

20 D. W. Fickel and R. F. Lobo, *J. Phys. Chem. C*, 2010, **114**, 1633-1640.

21 *US Pat.,* 4544538, 1985.

22 S. I. Zones, *J. Chem Soc., Faraday Trans.*, 1991, **87**, 3709-3716.

23 L. M. Ren, L. F. Zhu, C. G. Yang, Y. M. Chen, Q. Sun, H. Y. Zhang, C. J. Li, F. Nawaz, X. J. Meng and F. S. Xiao, *Chem. Commun.*, 2011, **47**, 9789-9791.

24 L. M. Ren, Y. B. Zhang, S. J. Zeng, L. F. Zhu, Q. Sun, H. Y. Zhang, C. G. Yang, X. J. Meng, X. G. Yang and F. S. Xiao, *Chin. J. Catal.*, 2012, **33**, 92-105.

25 W. Xu, Y. Yu, C. Zhang and H. He, *Chem. Commun.*, 2008, **9**, 1453-1457.

26 *US Pat.,* 0290963, 2010.

27 L. Ma, J. H. Li, H. Arandiyan, W. B. Shi, C. X. Liu and L. X. Fu, *Catal. Today*, 2012, **184**, 145-152.

28 L. Ma, Y. S. Cheng, G. Cavataio, R. W. McCabe, L. X. Fu and J. H. Li, *Chem. Eng. J.*, 2013, **225**, 323-330.

29 U. Deka, A. Juhin, E. A. Eilertsen, H. Emerich, M. A. Green, S. T. Korhonen, B. M. Weckhuysen and A. M. Beale, *J. Phys. Chem. C*, 2012, **116**, 4809-4818.

30 M. Zamadies, X. h. Chen and L. Kevan, *J. Phys. Chem.*, 1992, **96**, 2652-2657.

31 J. Dědeček, B. Wichterlová and P. Kubát, *Micropor. Mesopor. Mater.*, 1999, **32**, 63-74.

32 L. Xie, F. Liu, L. Ren, X. Shi, F.-S. Xiao and H. He, *Environ.Sci.Technol.*, 2013, **48**, 566-572.

33 G. A. V. Martins, G. Berlier, S. Coluccia, H. O. Pastore, G. B. Superti, G. Gatti and L. Marchese, *J. Phys. Chem. C*, 2007, **111**, 330-339.

34 L. Xu, A. P. Du, Y. X. Wei, Y. L. Wang, Z. X. Yu, Y. L. He, X. Z. Zhang and Z. M. Liu, *Micropor. Mesopor. Mater.*, 2008, **115**, 332-337.

35 L. L. Wu, V. Degirmenci, P. C. M. M. Magusin, N. J. H. G. M. Lousberg and E. J. M. Hensen, *J. Catal.*, 2013, **298**, 27-40.

36 Z.H. Li, W. Huang, Z.J. Zuo, Y.J.Song, K.C. Xie, *Chin. J. Catal.*, 2009, **30**, 171-177.

37 J. C. Wang, Z. Q. Liu, G. Feng, L. P. Chang and W. R. Bao, *Fuel*, 2013, **109**, 101-109.

38 R. T. Figueiredo, A. Martínez-Arias, M. L. Granados and J. L. G. Fierro, *J. Catal.*, 1998, **178**, 146-152.

39 L. Wang, J. R. Gaudet, W. Li and D. Weng, *J. Catal.*, 2013, **306**, 68-77.

40 F. Gao, E. D. Walter, N. M. Washton, J. Szanyi and C. H. F. Peden, *ACS Catal.*, 2013, **3**, 2083-2093.

41 H. Yahiro, Y. Ohmori and M. Shiotani, *Micropor. Mesopor. Mater.*, 2005, **83**, 165-171.